

Experimental and numerical investigation of an optimized airfoil for vertical axis wind turbines

Daniele Ragni

Delft University of Technology - DUWind

Carlos Simão Ferreira

Delft University of Technology - DUWind

Matthew Barone

*Sandia National Laboratories**

The present study addresses the experimental and numerical verification of the performance of a new airfoil design for lift driven vertical-axis wind-turbines (VAWT). The airfoil is obtained by a genetic algorithm optimization of the objective function proposed by Simão Ferreira and Geurts [19], which optimizes the aerodynamic performance of airfoils having a relatively larger thickness, providing with better structural stiffness compared to more slender NACA design. The work presents an experimental analysis of such improved performance of a 26% thick VAWT-optimized airfoil (DU12W262). The 2D flow velocity, pressure and aerodynamic loads are measured by combined use of Particle Image Velocimetry, wall-pressure sensors and wake rakes. Additionally, the airfoil surface pressure is determined by integrating the pressure equation from the experimental velocity field. Results are initially obtained with the airfoil in steady conditions, at Reynolds 3.5×10^5 , 7.0×10^5 and 1.0×10^6 with both free and forced (1%*c*) boundary layer transition. Xfoil simulations are employed for comparison to the experimental results, showing a good agreement in the linear range of angle of attack and a consistent lift/drag overestimation in the separated one. The experimental data are used as input for a numerical simulation of a 2D VAWT. CFD simulations of the airfoil are performed and validated against the experimental data. *NOTE: This is a draft and incomplete version of the paper, as the CFD simulations are yet not available. The full updated version of the paper will be available upon the conference.*

Nomenclature

I. Introduction

The recent development of off-shore wind-energy renewed the interest in the performance of in lift-driven vertical-axis wind-turbines VAWTs, with particular attention to floating installations (see Akimoto et al. [1], Paquette and Barone [16], Paulsen et al. [17]). In this respect, VAWTs present several geometrical advantages, which outperform their direct horizontal-axis competitors, which assessed their better feasibility for on-shore applications (see Sutherland et al. [22], Jamieson [11]). In particular, due to a better surface area distribution which grows with the turbine height instead of with the radius and to the possibility to install the generator at water level, VAWTs are better suited for densely spaced of floating turbine arrays. However, these advantages are counter-balanced by a more dynamic aerodynamics at the blade, rotor and wind-farm scales, which directly influence the cost of energy in four ways:

- Aerodynamic loading: impact in structure fatigue.
- Power produced: effective power converted with operation in yawed and turbulent flows.
- Wake development: recovery of stagnation enthalpy in the 3D wake development.

*Sandia National Laboratories is a multi-program laboratory managed and operated by Sandia Corporation, a wholly owned subsidiary of Lockheed Martin Corporation, for the U.S. Department of Energy's National Nuclear Security Administration under contract DE-AC04-94AL85000.

- Structural dynamics: blade deformation and dislocation, especially in floating conditions.

Within this framework, the achievement of an optimal compromise between aerodynamic performance and structural stiffness requires a multi-scale optimization, including both the blade, the rotor and the wind-farm scales. In the past decades, VAWT blades have typically been designed as geometric extrusion of symmetric airfoils, most notably belonging to the NACA 4 digits family, most notably NACA0012, NACA0015 and NACA0018 (see E. and Klimas [9] and Timmer [23]). Among the most complete works in designing and testing of VAWTs airfoils, stands out the research developed at the Sandia National Laboratories (see Klimas [13]) and at the Glasgow University (see Galbraith et al. [10]), primarily focusing on the steady and pitching performance of families of cambered airfoils, together with the studies of the Delft University of Technology for small scale VAWTs applications VAWTs (see Claessens [4]). More in detail, the research at the Sandia National Laboratories and at the Glasgow University achieved two relevant milestones: the determination of desirable section characteristics for lowering the cost of energy [13]; and the coupling of the airfoil design optimisation with a vorticity based model of the rotor [10], eliminating several of the incorrect assumptions of stream-tube models. The work of Klimas [13], citing the work of Sullivan [21], includes in the design drivers, the impact of stall regulation in thin airfoils (“*modest values of maximum lift coefficient with relatively sharp stall*”, [13]) together with the obvious reduction of airfoil drag (“*low zero lift drag coefficients, and [...] wide drag buckets*”, Klimas [13]). Complementary to that, the work of Galbraith et al. [10] integrates and extends the improvements at the airfoil scale in the modeling of the induction field developed by Jiang et al. [12] (see also Basuno et al. [2] and Coton et al. [6]). One of the main disadvantages of the usage of thin airfoils in VAWTs applications consists on their reduced structural stiffness, compensated by an increased cost of the material mass and the reinforcement needed for the construction of the blades. The employment of such thin airfoils is mainly dictated by the fact that most of VAWTs design studies are still based on the aerodynamic efficiency of HAWTs, that is the glide ratio of the airfoil: $\frac{C_l}{C_d}$, as one of the guidelines for the generation of an optimal airfoil shape. The work of Simão Ferreira and Geurts [19], following the ones of Wilson [25], Coene [5], Madsen [14, 15], Simão Ferreira [18] and Simão Ferreira and Scheurich [20] (see also Jamieson [11] presents instead an objective function for the aerodynamic optimization of VAWTs airfoils based on the first principle of the 2D VAWT aerodynamics. In particular, the generation of the wake by variation of the bound circulation on the airfoil and the dependency of the latter with solidity and airfoil lift slope is used as a guideline to the design. The particular derivation of the function demonstrates that high turbine performance can be obtained with thicker airfoils, due to the proportionality of the airfoil lift slope to its thickness. In the present study a new airfoil is designed from the optimization procedure according to Simão Ferreira and Geurts [19]. From the procedure which allows obtaining a relatively thicker airfoil with good aerodynamic performance, the manuscript focuses on an experimental and numerical investigation to validate the simulated airfoil lift and drag performance.

II. Design of the DU12W262 airfoil

The DU12W262 airfoil shape is the result of an optimization procedure for aerodynamic and structural performance (Simão Ferreira and Geurts [19]). Selected from an initial population of airfoils through a genetic algorithm, the shape is evaluated via two objective functions. The optimization algorithm used in this work was developed by de Oliveira [8] and Simão Ferreira and Geurts [19]; it is constructed around the NSGA-II algorithm as implemented in MATLAB R2011. The most relevant elements of the algorithm are described by de Oliveira [8]. The structural objective function was defined as the bending stiffness in flap-wise direction of the airfoil per wall-thickness. The bending stiffness is defined in reference to the centroid of the airfoil. The resulting DU12W262 airfoil is presented in Figure 1.

III. Experimental setup

A. Airfoil realization and wind tunnel measurements

The DU12W262 airfoil shape has been manufactured into an aluminium model of chord $c = 0.25m$, span $s = 1.25m$, aspect ratio $AR = s/c = 5$ and thickness $t/c = 26.2\%$, with a mass of $34.7kg$. The model has been vertically installed in the closed-circuit low-turbulence wind-tunnel (LTT) of the TU Delft laboratories, in an octagonal test section $1.80m$ wide, $1.25m$ high and $2.60m$ long determining a blockage ratio from 3.6% to 4.7% in the range from -20 to 20 degrees angles of attack. With a contraction ratio of 17.6 , the

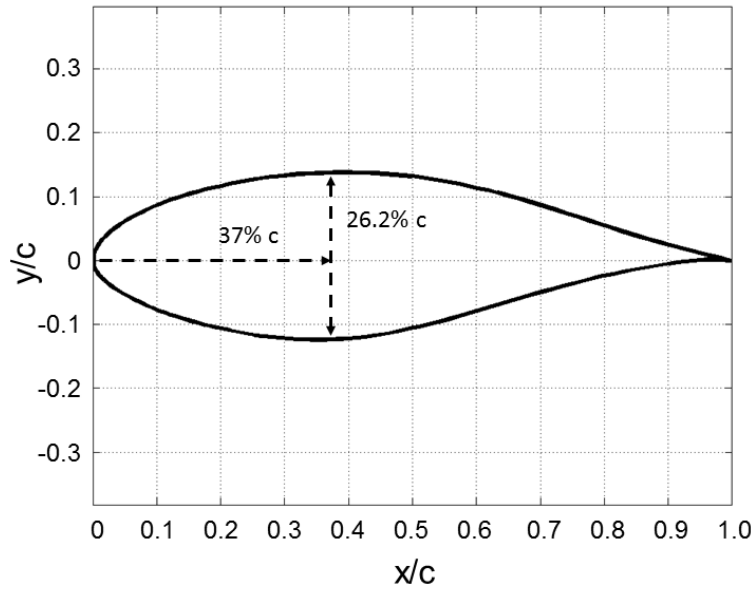


Figure 1: DU12W262 airfoil geometry

wind-tunnel can reach a maximum wind-speed of $120m/s$ and a turbulence level ranging within 0.015% to 0.07% with wind speeds from $10m/s$ to $75m/s$ (from hot wire anemometry profiles with low-pass filter at $50kHz$). Steady-flow measurements have been performed by acquiring several angles of attack at Reynolds $3.5 * 10^5$, $7.0 * 10^5$ and 10^6 , with wind-tunnel speeds ranging from 20 to $60m/s$. Pitching tests have been performed at a Reynolds number of $7.0 * 10^5$, for respectively $\pm 5^\circ$, $\pm 10^\circ$, $\pm 20^\circ$ amplitude variation, with reduced frequencies ranging from $k = 0.07$ to $k = 0.11$. The obtained cycles shapes results from the linear actuator imposing a quasi-linear acceleration/deceleration on the actuating rod. The obtained shape profiles, though not sinusoidal, allowed for a better response of the system to vibrations and a lower inertial force effect on the wind-tunnel walls.

B. PIV diagnostic apparatus

The flow velocity fields at different angles of attack have been obtained by performing $2D$ double-camera PIV measurements. The velocity results have been used to compute pressure and aerodynamic loads for both steady and pitching configurations (van Oudheusden et al. [24], D. Ragni and Scarano [7]). Seeding particles have been produced by a SAFEX fog machine able to generate droplets with a median diameter of $\approx 1\mu m$. The seeding particles have been injected downstream the model, determining a uniform and homogeneous concentration at the test section after flow recirculation in the closed circuit. Laser illumination is provided at the airfoil middle-span by a Quantel CFR200 Nd:YAG laser ($200mJ/pulse$), and conveyed through laser optics to form a laser sheet of approximately $2mm$ thickness at the field of view (FOV). In both steady and pitching conditions, a double-sided illumination setup has been used in order to reduce the effect of laser shadow (Figure 2). The double-sided illumination has been obtained by splitting the laser beam into two beams (B1, B2 in Figure 2) through a cubical beam splitter. Two CCD LaVision Imager Pro LX cameras of $4872 * 3248 \text{ pix}^2$ with two Nikon lenses of $105mm$ focal length and aperture $f\#5.6$ are combined to form a planar field of view encompassing the airfoil shape and perpendicular to the span-wise direction (section plane). Additionally, the usage of two cameras allow seeing both top and bottom airfoil surfaces, mitigating the prospective effect encountered with just one camera. Image acquisition and processing has been carried out by LaVision DaVis 8.1 software. For each angle of attack, approximately 200 images have been captured and processed by average correlation, with a window size of $24 * 24 \text{ pix}^2$ and 50% overlap, giving a vector spacing of $0.9mm$. The images have been combined into a single field of view (FOV) encompassing the airfoil. In the pitching configuration, the same setup has been employed; however, the acquisition has been synchronized with the phase of the pitching motion (phase-locked) through the use of a Stanford acquisition system and a mechanical trigger installed on the pitching axis. Phase-delaying the signal with respect to the

reference delay coming from the mechanical trigger allowed acquiring images corresponding to the different angles of attack in motion.

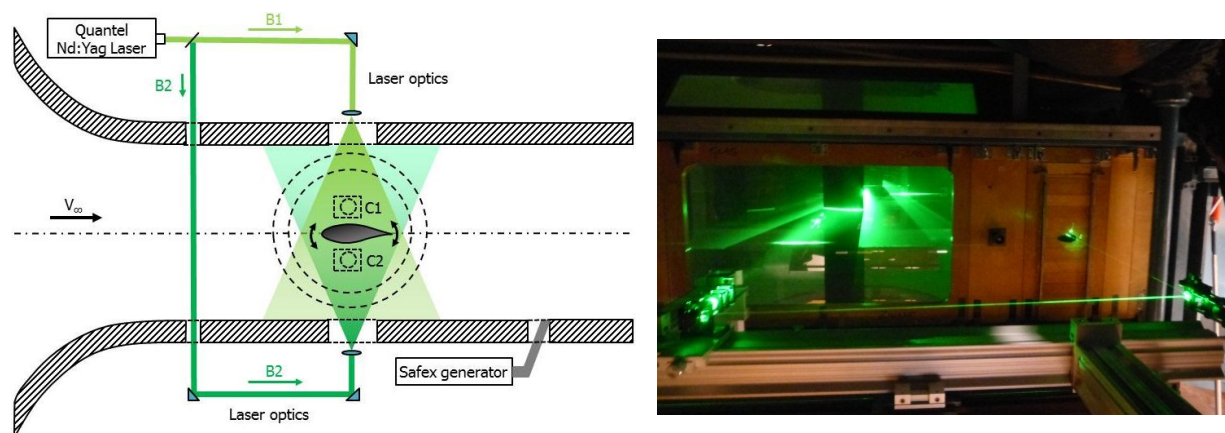


Figure 2: Top view of the PIV apparatus (left), B1 B2: illumination beams, C1 C2 cameras; realization of the PIV setup (right)

Different PIV velocity fields have been acquired to visualize the flow and to obtain the forces to be compared to the pressure sensors (wall-tunnel pressure probes and wake-rake Pitot tubes).

IV. Pressure and load determination methodology

The aerodynamic loads are obtained for both steady and pitching configurations. In the steady airfoil configuration a series of 44 (22 per wall, variable spacing from 17.8cm to 4.5cm , total length of 2.095m) wind-tunnel wall-pressure orifices have been employed to obtain the static pressure distribution on the wind-tunnel mid-span, integrated into lift. Additionally, a wake rake constituted of 64 Pitot probes (variable spacing from 3mm to 24mm , total length of 0.516m) has been employed to measure drag at the different angles of attack. The lift coefficient has been also obtained through the PIV load determination as in (D. Ragni and Scarano [7]). Wake rake results have been used for the determination of the drag force for the steady case.

The pressure field is directly derived from the PIV velocity fields. Except for the airfoil boundary layer and for the airfoil wake, the flow is potential, therefore the Bernoulli equation can be used to directly evaluate the obtain to directly evaluate the pressure coefficient C_p from the local velocity V [m/s] and the free stream one V_∞ [m/s] at the boundary of the FOV (except wake):

$$c_p = 1 - \left(\frac{|\bar{V}|}{V_\infty} \right)^2 \quad (1)$$

In the airfoil wake, the flow is viscous and the Bernoulli equation is not valid, therefore the pressure in the FOV (except boundary) is computed from the integration of the Navier-Stokes pressure gradient:

$$\frac{\bar{\nabla} p}{p} = -\rho \left(\frac{\partial \bar{V}}{\partial t} + \bar{V} \cdot \bar{\nabla} \bar{V} \right) + \bar{\nabla} \bar{\tau} \quad (2)$$

V. Experimental results

A. Steady airfoil results

The airfoil flow results pertaining to the steady flow configuration are obtained by fixing the angle of attack through a rotating mechanism integrated with the wind-tunnel upper wall. PIV velocities fields for different angles of attack ranging from -20° to $+20^\circ$ are acquired at two Reynolds numbers $Re = 10^6$ and $Re = 7 \cdot 10^5$. A sequence of five angles of attack (ensemble averaged results) are here presented as normalized velocity field (Figure 3), normalized vorticity field (Figure 4), and pressure field (Figure 5). The variability of the airfoil performance with different Reynolds numbers has been investigated in more detail by use of the wind-tunnel

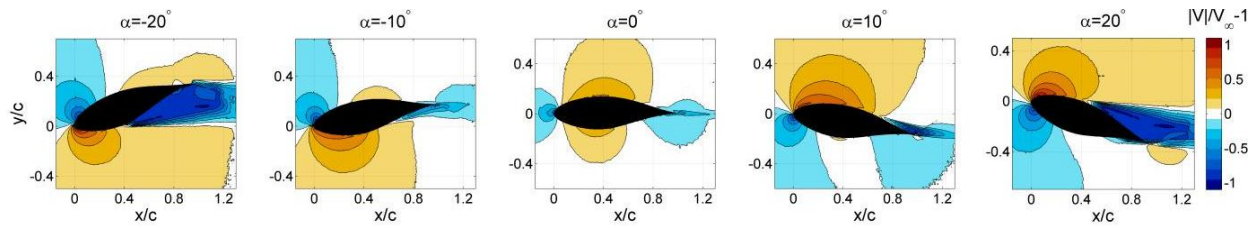


Figure 3: PIV normalized velocity magnitude (free-stream reference), steady airfoil configuration, free transition, $Re = 10^6$

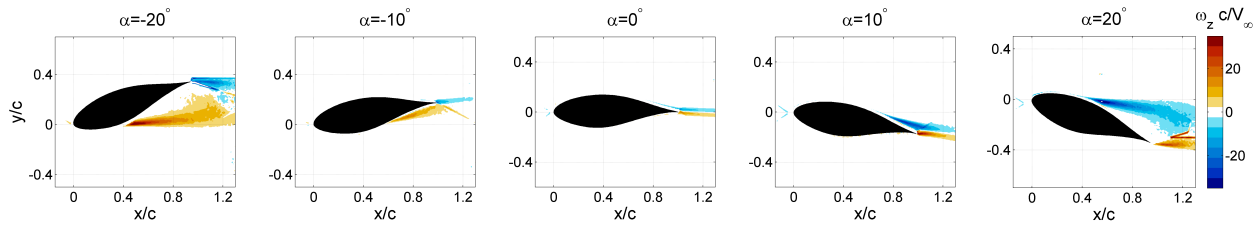


Figure 4: PIV normalized vorticity magnitude, steady airfoil configuration, free transition, $Re = 10^6$

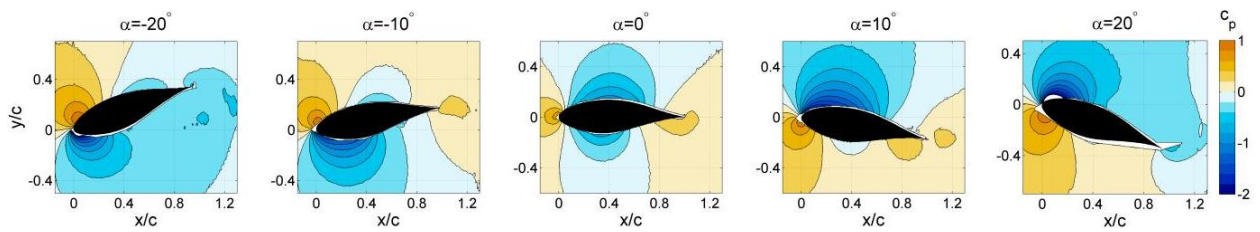


Figure 5: PIV pressure coefficient, steady airfoil configuration, free transition, $Re = 10^6$

wall-pressure sensors. Figure 6 presents the airfoil lift coefficients for different Reynolds numbers, in both free (left) and forced boundary layer transition (right) configurations as obtained from integration of the wind-tunnel wall-pressure. Figure 6 (left) shows a relatively low effect of the Reynolds number in the performance of the airfoil under free transition, mainly evidenced by a slight slope variation induced in the lift curve. With decreasing Reynolds number, a shift of the curve towards negative lift is noticeable. The configuration with forced transition in Figure 6 (right) presents a similar behaviour with the change in Reynolds number, although the effect of the fully turbulent flow in the airfoil delays stall to respectively $+15^\circ$ and -20° angles of attack, in comparison to $+10^\circ$, -12° in the clean configuration. These results are the consequence of the presence of a laminar separation bubble in the free transition case, which is no longer present in the forced transition case. The maximum lift coefficient at $Re > 7 * 10^5$ is also reduced from the free to the forced transition configuration, decreasing from 1.2 to 0.95. The drag curves in Figure 7 are obtained with the wake-rake installed downstream the airfoil. The results in Figure 7 further confirms the effect of the change in Reynolds number in the airfoil under free and forced transition. The drag coefficient in the free transition configuration persists at an almost constant value in the attached flow range of angles of attack $+10^\circ$, -12° (cfr. Figure 7), while in the forced transition the range restricts to half. The performance of the airfoil has been subsequently compared to the results obtained by Xfoil simulations. In particular Figure 8 (top-left) shows the lift coefficient distribution integrated from the velocity data compared to the one obtained by integration of the wind-tunnel wall-pressure profile and Xfoil results. Concurrently, in Figure 8 (top-right), the experimental drag coefficient is compared to the one obtained from the Xfoil simulations. Due to the usual lower accuracy of the drag coefficient as computed from PIV, the experimental results are here obtained from integration of the total pressure measured by a wake rake of Pitot tubes, installed at almost two chords downstream of the airfoil profile. Figure 8 shows the asymmetrical load distribution for positive and negative angles, with maximum lift obtained at $+9^\circ$, -10° . The Xfoil simulations agree for most of the range of angles, over-predicting lift for angles higher than $+10^\circ$. Few differences are noticeable for the two investigated Reynolds numbers, which are primarily detectable on the measured drag coefficient Figure 8 (top-right). Similarly to the lift coefficient distribution, the drag coefficient shows typically higher values reported in the separated zones than in the Xfoil simulations, fact ascribed to the way the boundary layer transition is obtained in the experiment with respect to the Xfoil simulations. The calculations are further carried on for the forced transition test cases in Figure 8 (bottom) and compared again to the wall-pressure probes and to the wake rake results. The resulting curves here show a much higher over prediction of the experimental results compared to the Xfoil simulations. The forced transition is experimentally obtained through the use of zig-zag tape of $0.4mm$ thickness and $6mm$ pitch and positioned at 2% chord. Although the height of the zig-zag tape is in the min/max height range as specified by Braslow and Knox [3] from $0.07mm$ to $0.47mm$ the relatively high value might justify the discrepancies with the Xfoil simulations, especially in the separated region. Similarly, in the XFOIL simulation, the airfoil transition is imposed at 2% chord and the results computed. The airfoil sensitivity to the presence of fully turbulent flow is relevant, especially with respect to the free-transition case. No-hysteresis phenomena are noted in any of the steady change of angles of attack.

VI. Evaluation of the performance of the airfoil on a 2D VAWT

Figure 9 presents the simulated power coefficient (C_P) for a three bladed VAWT as a function of tip speed ratio (λ) and solidity for the DU12W262; the simulations are based on the experimental airfoil polar for the DU12W262 (Figures 6 and 7).

VII. Conclusions

The work aimed at testing and simulating an optimized airfoil for VAWTs, design accordingly to the objective function proposed by Simão Ferreira and Geurts [19]. The designed airfoil performance has been tested for a range of Reynolds numbers of the order of 0.7 to 1 million, relevant for wind-energy applications. The experimental wind-tunnels results served to validate numerical predictions; the numerical and experimental results matched well for the $C_l(\alpha)$ curve, but the numerical results for $C_d(\alpha)$ under-predict the experiments. As the airfoil is optimized with the use of a small separation bubble for transition, small variations between numerical and experimental model can justify this difference in drag without significant difference in lift. The results also confirm the suitability of using Particle Image Velocimetry for the study

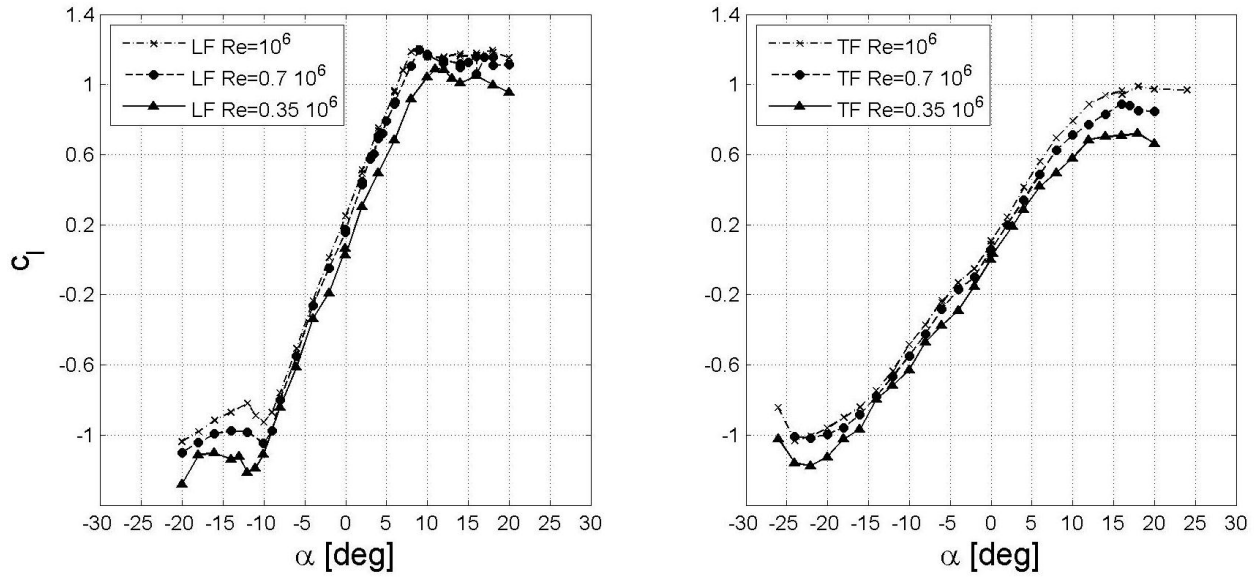


Figure 6: Lift coefficient (experimental) for the DU12W262 under free (left) and forced (right) transition

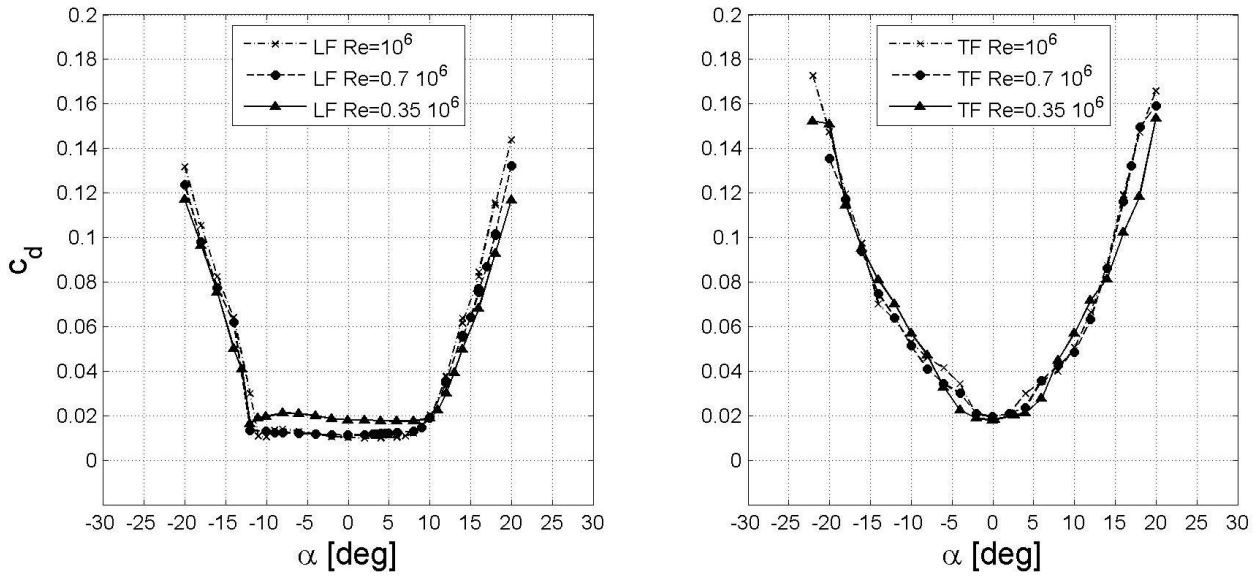


Figure 7: Drag coefficient (experimental) for the DU12W262 under free (left) and forced (right) transition

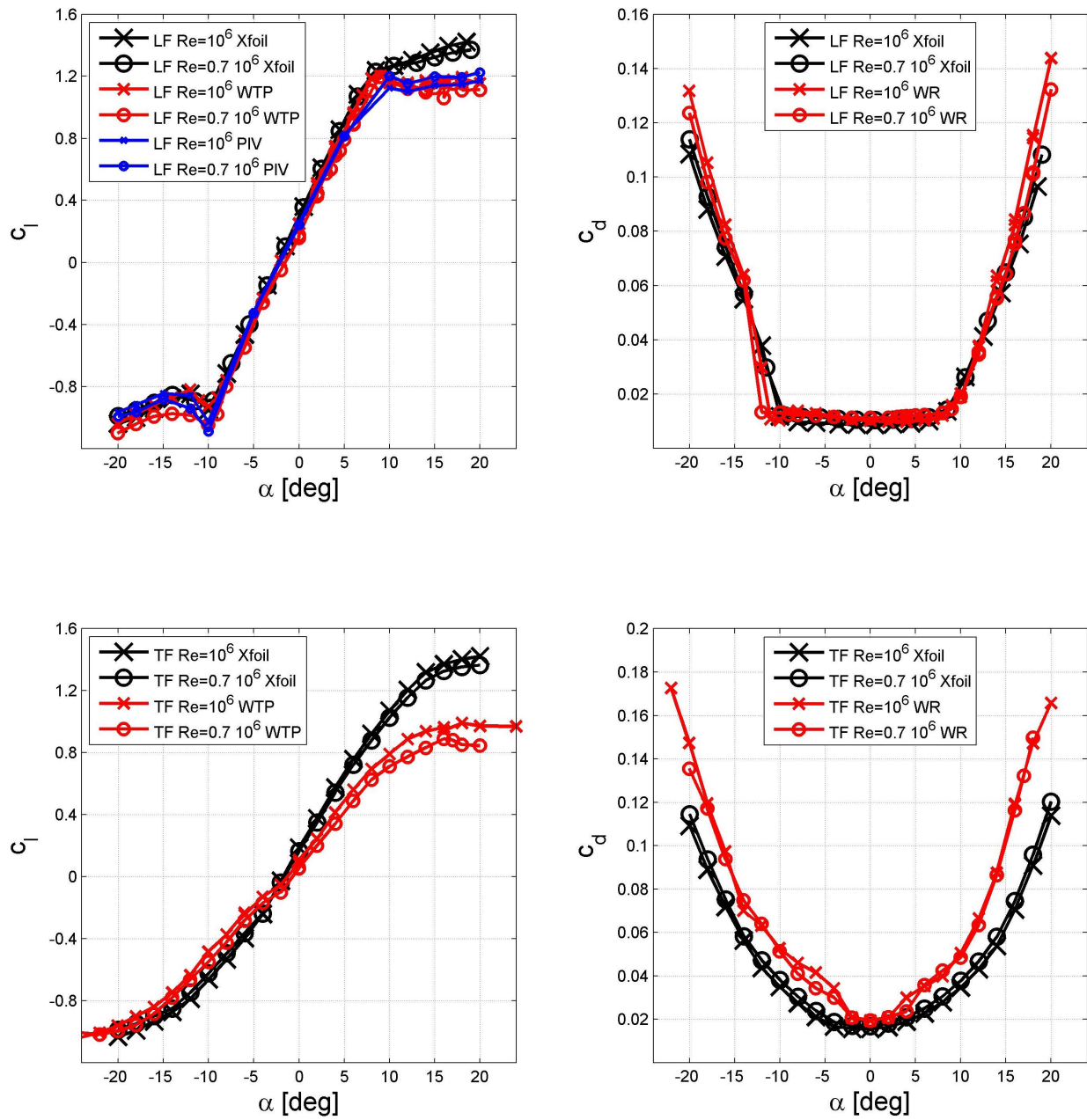


Figure 8: c_l and c_d obtained by tunnel pressure probes, wake rake, Xfoil simulations, and from PIV load determination (free transition)

- ⁹ E., R. and Klimas, P. C. (1981). Aerodynamic characteristics of seven symmetrical airfoil sections through 180-degree angle of attack for use in aerodynamic analysis of vertical axis wind turbines. Technical Report SAND81-2114, Sandia National Laboratories.
- ¹⁰ Galbraith, R., Coton, F., and Dachun, J. (1992). Aerodynamic design of vertical axis wind turbines. Technical Report GU Aero 9246, University of Glasgow.
- ¹¹ Jamieson, P. (2011). *Innovation in wind turbine design*. John Wiley & Sons.
- ¹² Jiang, D., F.N.Coton, and Galbraith, R. M. (1991). A fixed vortex model for vertical axis wind turbines including unsteady aerodynamics. *Wind Engineering*, 15(6):348–360.
- ¹³ Klimas, P. C. (1984). Tailored airfoils for vertical axis wind turbines. Technical Report SAND84-1062, Sandia National Laboratories and United States. Dept. of Energy.
- ¹⁴ Madsen, H. A. (1983). On the ideal and real energy conversion in a straight bladed vertical axis wind turbine. Technical report, Institute of Industrial Constructions and Energy Technology - Aalborg University Centre.
- ¹⁵ Madsen, H. A. (1985). The actuator cylinder: a flow model for the vertical axis wind turbine. In *Proceedings of the 7th British Wind Energy Association Conference*, pages 147–154.
- ¹⁶ Paquette, J. and Barone, M. (2012). Innovative offshore vertical-axis wind turbine rotor project. *EWEA 2012 Annual Event, Copenhagen, Denmark*.
- ¹⁷ Paulsen, U. S., Vita, L., Madsen, H. A., Hattel, J., Ritchie, E., Leban, K. M., Berthelsen, P. A., and Carstensen, S. (2012). 1st Deepwind 5MW baseline design. *Energy Procedia*, 24(0):27 – 35.
- ¹⁸ Simão Ferreira, C. (2009). *The near wake of the VAWT: 2D and 3D views of the vawt aerodynamics*. PhD thesis, Delft University of Technology. ISBN/EAN:978-90-76468-14-3.
- ¹⁹ Simão Ferreira, C. and Geurts, B. (2013). Derivation of an objective function for aerofoil optimisation for the vertical axis wind turbine. *submitted to Wind Energy*. in review.
- ²⁰ Simão Ferreira, C. and Scheurich, F. (2013). Demonstrating that power and instantaneous loads are decoupled in a vertical axis wind turbine. *Wind Energy*. Published Online.
- ²¹ Sullivan, W. (1979). Economic analysis of darrieus vertical axis wind turbine systems for the generation of utility grid electric power - vol. 2: The economic optimization model. Technical report, Sandia National Laboratories.
- ²² Sutherland, H. J., Berg, D. E., and Ashwill, T. D. (2012). A retrospective of vawt technology. *Sandia Report SAND2012-03044 Sandia National Laboratories: Livermore, CA*.
- ²³ Timmer, W. (2008). Two-dimensional low-reynolds number wind tunnel results for airfoil naca 0018. *Wind Engineering*, 32(6):525–537.
- ²⁴ van Oudheusden, B., Scarano, F., Roosenboom, E., Casimiri, E., and Souverein, L. (2007). Evaluation of integral forces and pressure fields from planar velocimetry data for incompressible and compressible flows. *Experiments in Fluids*.
- ²⁵ Wilson, R. (1978). Vortex sheet analysis of the giromill. *Journal of Fluids Engineering*, 100(3):340–342.